CXCR4/CXCL12-mediated entrapment of axons at the injury site compromises optic nerve regeneration

Alexander M. Hilla[a] [ID], Annemarie Baehr[a], Marco Leibinger[a], Anastasia Andreadaki[a] [ID], and Dietmar Fischer[a,1] [ID]

[a]Department of Cell Physiology, Faculty of Biology and Biotechnology, Ruhr University, 44780 Bochum, Germany

Regenerative failure in the mammalian optic nerve is generally attributed to axotomy-induced retinal ganglion cell (RGC) death, an insufficient intrinsic regenerative capacity, and an extrinsic inhibitory environment. Here, we show that a chemoattractive CXCL12/CXCR4-dependent mechanism prevents the extension of growth-stimulated axons into the distal nerve. The chemokine CXCL12 is chemoattractive toward axonal growth cones in an inhibitory environment, and these effects are entirely abolished by the specific knockout of its receptor, CXCR4 (CXCR4$^{-/-}$), in cultured regenerating RGCs. Notably, 8% of naïve RGCs express CXCL12 and transport the chemokine along their axons in the nerve. Thus, axotomy causes its release at the injury site. However, most osteopontin-positive α-RGCs, the main neuronal population that survives optic nerve injury, express CXCR4 instead. Thus, CXCL12-mediated attraction prevents growth-stimulated axons from regenerating distally in the nerve, indicated by axons returning to the lesion site. Accordingly, specific depletion of CXCR4 in RGC reduces aberrant axonal growth and enables long-distance regeneration. Likewise, CXCL12 knockout in RGCs fully mimics these CXCR4$^{-/-}$ effects. Thus, active CXCL12/CXCR4-mediated entrapment of regenerating axons to the injury site contributes to regenerative failure in the optic nerve.

axon regeneration | optic nerve | CNS | CXCR4 | CXCL12

Retinal ganglion cells (RGCs) convey the visual input from the eye through the optic nerve and optic tract into the brain's target regions. As typical neurons of the central nervous system (CNS), mammalian RGCs lose most of their capability to regrow injured axons after birth (1, 2), leading to an irreversible functional loss after optic nerve damage. To date, regenerative failure has been mainly attributed to three leading causes: 1) axotomy-induced apoptosis of RGCs, 2) the low intrinsic capacity to regrow axons, and 3) the external inhibitory environment with CNS myelin and glial scar proteins (3, 4).

One widely used approach to delay axotomy-induced RGC degeneration and activate the intrinsic regenerative capacity of injured axons is inflammatory stimulation (IS) in the eye induced by a lens injury, intravitreal Pam$_3$Cys, or zymosan injection (5–7). IS leads to the expression and release of CNTF, LIF, and IL-6 from retinal astrocytes and Müller cells (8–10), which directly interact with RGCs and activate neuroprotective/regenerative signaling such as the JAK/STAT3 pathway (8, 9, 11, 12). IS, therefore, enables moderate axon regeneration beyond the lesion site of the optic nerve. Although combinatorial strategies, together with measures overcoming the inhibitory CNS environment synergistically, further improve IS-mediated optic nerve regeneration (13–17), the overall outcome remains mostly unsatisfactory. Thus, additional unknown mechanisms besides neurodegeneration, low intrinsic capacity, and the inhibitory environment might contribute to optic nerve regeneration failure.

The chemokine receptor CXCR4, a seven-transmembrane G protein–coupled receptor, is expressed in embryonic and adult neurons (18–20). We have recently shown that this receptor is also expressed in the somata and axons of adult rat RGCs (18). Next to its role as a coreceptor for HIV entry and cancer-cell migration/proliferation (21, 22), CXCR4 is reportedly involved in neurogenesis

and axonal pathfinding during the embryonal development of RGCs (20, 23, 24). CXCR4 regulates different signaling pathways upon binding its ligand CXCL12 (also known as stromal cell–derived factor 1, SDF-1), which is part of the chemokine family of chemotactic cytokines in the immune system involved in the attraction of lymphocytes (25, 26). CXCL12 is also reportedly expressed by some CNS neurons, astrocytes, and microglia (19, 27–30). As the CXCR4/CXCL12 axis is highly conserved between different species (31) and involved in axonal pathfinding during embryonal development of RGCs (20, 32), we speculated that CXCR4 expression in adult RGCs might also play a role in the regenerative processes of mature axons.

The current study shows that growth-stimulated axons of RGCs are actively attracted and entrapped at the lesion site of the optic nerve by a CXCL12/CXCR4-dependent mechanism. CXCL12 is expressed in a subpopulation of RGCs and axonally transported, implying its release at the injury site. A different RGC subpopulation expressed CXCR4, causing axons in the distal nerve to return to the injury site. Specific depletion of CXCR4 or CXCL12 in RGCs abolished aberrant growth. It enabled long-distance regeneration in the optic nerve, with some axons reaching the optic chiasm 3 wk after injury. Thus, active CXCL12/CXCR4-mediated entrapment markedly compromises axon extension into the distal optic nerve and contributes to regenerative failure in the optic nerve.

Significance

Retinal ganglion cell (RGC) axons in the optic nerve convey visual information from the eye to the brain. Injury causes permanent functional loss as axons cannot regenerate. This failure is generally attributed to an insufficient intrinsic regenerative capacity, the extrinsic inhibitory environment, and RGC death. Here, we show that a chemoattractive CXCL12/CXCR4-dependent mechanism entraps growth-stimulated axons at the lesion site, thereby limiting axon extension in the nerve. Accordingly, specific depletion of either CXCR4 or CXCL12 in growth-stimulated RGCs releases entrapped axons and markedly enhances nerve regeneration at long distances. Thus, active CXCL12/CXCR4-mediated attraction to the injury site represents a mechanism preventing central nervous system (CNS) axon regeneration. Moreover, treatments targeting CXCL12/CXCR4 signaling may be promising approaches to improve CNS repair.

NEUROSCIENCE

Results

CXCR4 Is Expressed in a Subpopulation of α-RGCs. We previously showed CXCR4 expression in adult RGCs (18). Quantification of immunohistochemically stained rat retinal flatmounts revealed, however, that only about 30% of RGC somata were CXCR4 positive (Fig. 1 *A* and *C*). CXCR4 was also clearly detectable in retinal axons (Fig. 1*A*) and about 30% of all neurofilament-positive fibers in optic-nerve cross-sections (Fig. 1 *B* and *C*). Murine retinae showed similar numbers of CXCR4-positive RGCs (27.5% ± 2.1%, *n* = 4) (Fig. 1*D*), and in this species, the specificity of the CXCR4 staining could be confirmed by inducing an RGC-specific knockout of the receptor (CXCR4$^{-/-}$). To this end, CXCR4-floxed mice received an intravitreal injection of AAV2-Cre-recombinase (AAV2-Cre, leading to the knockout in about 85% of RGCs) or AAV2-GFP (control, CXCR4$^{+/+}$) several wk before tissue isolation (Fig. 1 *E*–*G* and *SI Appendix*, Fig. S1*A*). Immunohistochemical and Western blot analysis showed a clear, detectable CXCR4 signal in controls but not in Cre-expressing (CXCR4$^{-/-}$) RGCs (Fig. 1 *E*–*G* and *SI Appendix*, Fig. S1*A*). Further analysis using double immunohistochemical staining revealed the vast majority of CXCR4-positive RGCs (97% ± 0.3%, *n* = 4) coexpressed osteopontin (OPN), a marker for the α-RGC subtype (Fig. 1*H*). However, not all OPN-positive RGCs measurably coexpressed CXCR4 and therefore some α-RGCs may not be sensitive to

CXCL12. Significantly, α-RGCs are characterized by the highest resilience toward axotomy-induced RGC death and a high intrinsic regenerative capacity (33). Therefore, almost all axons usually regenerating in the optic nerve after PTEN knockout belong to this subtype (33).

Conditional CXCR4 Knockout Enables Long-Distance Regeneration of Growth-Stimulated RGCs. We next accessed the relevance of endogenous CXCR4 in RGCs for optic nerve regeneration. As described above, we generated animals with CXCR4$^{-/-}$ or CXCR4$^{+/+}$ RGCs by injecting either AAV-Cre or AAV-GFP into CXCR4-floxed mice. After 3 wk, mice were subjected to optic nerve crush (ONC) or ONC with inflammatory stimulation (ONC/IS). Compared to CXCR4$^{+/+}$ controls, which showed only a few short axons in the distal nerve segment 3 wk after injury, regeneration was slightly but nonsignificantly higher in animals with CXCR4$^{-/-}$ RGCs determined at 1.5 mm distal to the lesion site (Fig. 2 *A* and *B*). The average value of the longest axons in nerves was also slightly but nonsignificantly increased in CXCR4$^{-/-}$ RGCs (1.33 ± 0.14 mm) compared to CXCR4$^{+/+}$ controls (0.91 ± 0.07 mm). Nevertheless, these effects were low and remained much below the axon numbers measured after axon growth–stimulating IS in CXCR4$^{+/+}$ animals (Fig. 2 *C* and *D*). However, together with IS, RGC-specific CXCR4 depletion markedly increased axon numbers at distances >1.5 mm
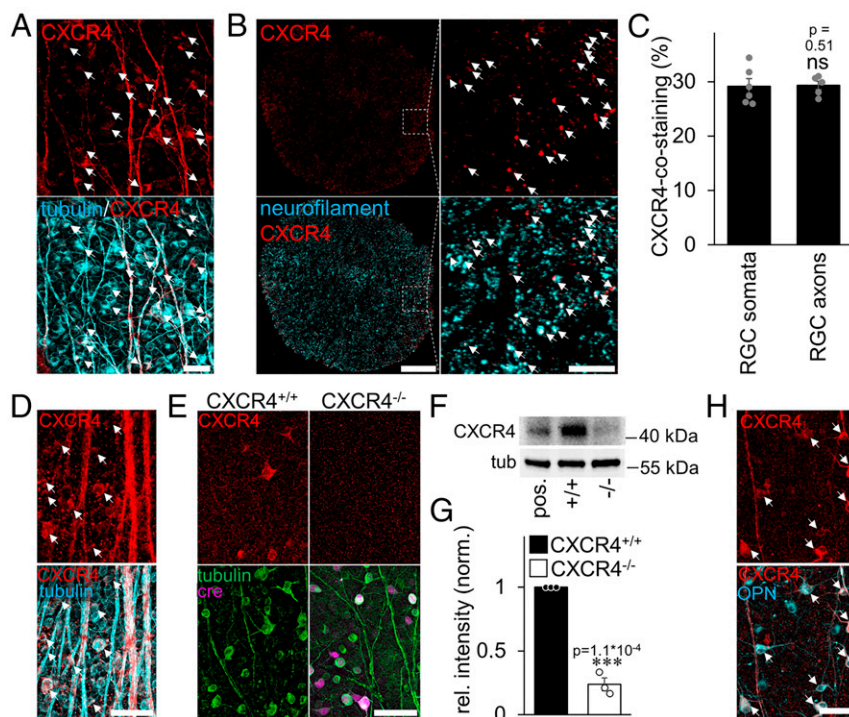
Fig. 1. CXCR4 expression in rodent retina and optic nerve. (*A*) Immunohistochemical staining of CXCR4 (red) in rat retinal wholemounts shows a distinct expression of the receptor in the somata and axons of βIII-tubulin–positive RGCs (cyan). White arrows highlight double-positive RGCs. (Scale bar, 50 μm.) (*B*) Rat optic nerve cross-sections show CXCR4-positive signals (red). Magnification (*Right*) reveals the localization of CXCR4 in neurofilament-positive axons (cyan). Most of the double-positive axons have been highlighted by white arrows. (Scale bars, 100 μm [overview] and 20 μm [magnification].) (*C*) Quantification of CXCR4-positive RGC somata and axons from pictures, as in *A* and *B*, reveal the expression of the receptor in a subpopulation of RGCs. Bars represent means ± SEM for at least *n* = 5 retinae and optic nerves per group; dots represent the single values per group. Treatment effects: ns: nonsignificant by χ^2 test. (*D*) Immunohistochemical staining of CXCR4 (red) in retinal wholemounts of mice show basal staining upon signal amplification in somata (white arrows) and axons of βIII-tubulin–positive RGCs (cyan). (Scale bar, 50 μm.) (*E*) Triple staining of retinal wholemounts shows expression of CXCR4 (red, arrows) in RGCs (green) of wild-type mice (CXCR4$^{+/+}$), while signals were absent in AAV-Cre–transduced CXCR4-floxed RGCs (CXCR4$^{-/-}$) 5 wk after intravitreal injection and 2 wk after ONC. The *Right* panel shows an area of lower transduction, and the arrow indicates a remaining single CXCR4-positive RGC. (Scale bar, 50 μm.) (*F*) Western blot of retinal lysates from axotomized mice: RGC-specific CXCR4 depletion by intravitreal AAV-Cre injection ($^{-/-}$)–reduced CXCR4 expression compared to respective controls ($^{+/+}$). βIII-tubulin served as a loading control. HEK293 cells overexpressing CXCR4 served as the positive control (pos.) and verified the signal's specificity. (*G*) Densitometric quantification of CXCR4 relative to βIII-tubulin and normalized to control Western blot as depicted in *F*. Bars represent means ± SEM for *n* = 3 retinae per group; dots represent the single values per group. Treatment effects: ***P < 0.001 by Student's *t* test. (*H*) Double staining of retinal wholemount treated as *E* shows coexpression (white arrows) of CXCR4 (red) and OPN (cyan), a marker for α-RGCs. (Scale bar, 50 μm.)
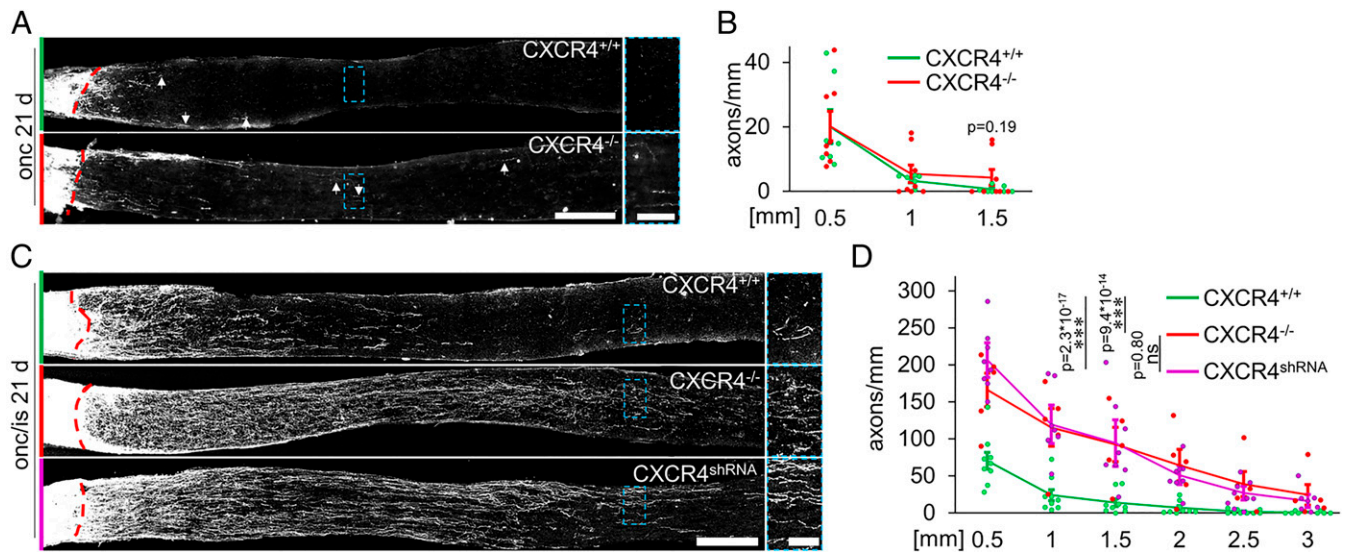
Fig. 2. Conditional CXCR4$^{-/-}$ potentiates optic nerve regeneration. (*A*) Longitudinal optic nerve sections with CTB-labeled, regenerating axons 21 d after optic nerve crush (onc). Nerves were isolated from CXCR4-floxed mice that had received intravitreal injection of either AAV-Cre to induce the knockout (CXCR4$^{-/-}$) in RGCs or AAV-GFP for respective controls (CXCR4$^{+/+}$). The dashed red line indicates the injury site, and arrows mark the longest regenerating axons. The dashed blue boxes indicate the magnified area (*Right*). (Scale bars, 250 μm [overview] and 50 μm [magnification].) (*B*) Quantification of axons extending more than 0.5, 1, and 1.5 mm beyond the injury site from groups described in *A*. Values represent means ± SEM for seven to eight mice per experimental group with five evaluated sections per mouse (CXCR4$^{+/+}$: $n = 7$; CXCR4$^{-/-}$: $n = 8$). Dots represent single values of each animal. (*C*) Longitudinal optic nerve sections with CTB-labeled regenerating axons 21 d after ONC and inflammatory stimulation (onc/is). Nerves were isolated from mice with CXCR4$^{+/+}$ RGCs, CXCR4$^{-/-}$ RGCs, or RGCs with a viral CXCR4 knockdown (CXCR4^{shRNA}). The dashed red line indicates the injury site. The dashed blue boxes indicate the magnified area (*Right*). (Scale bars, 250 μm [overview] and 50 μm [magnification].) (*D*) Quantification of regenerating axons extending indicated distances beyond the injury site described in *C*. IS-mediated optic nerve regeneration was similarly potentiated by CXCR4$^{-/-}$ or CXCR4^{shRNA} treatment compared to CXCR4$^{+/+}$. Values represent means ± SEM for 5 to 9 mice per experimental group and 5 sections per animal (CXCR4$^{+/+}$: $n = 9$; CXCR4$^{-/-}$: $n = 5$; CXCR4^{shRNA}: $n = 8$). Dots represent single values of each animal. Treatment effects: ***$P < 0.001$; ns: nonsignificant by two-way ANOVA with Holm–Šídák post hoc test.

more than 10-fold compared to IS in CXCR4$^{+/+}$ animals (Fig. 2 *C* and *D*), with many axons reaching distances longer than 3 mm. No axons were detected in the optic chiasm, verifying the absence of spared fibers (34). We also tested whether an shRNA-mediated CXCR4 knockdown approach can reach similar effects in wild-type animals. After the verification of the shRNA efficacy in cell culture and in vivo (*SI Appendix*, Fig. S1*B–E*), intravitreal injection of an AAV2 carrying this construct (AAV-CXCR4^{shRNA}) 3 wk before ONC/IS fully mimicked the beneficial effect of RGC-specific CXCR4 depletion on optic nerve regeneration (Fig. 2 *C* and *D*).
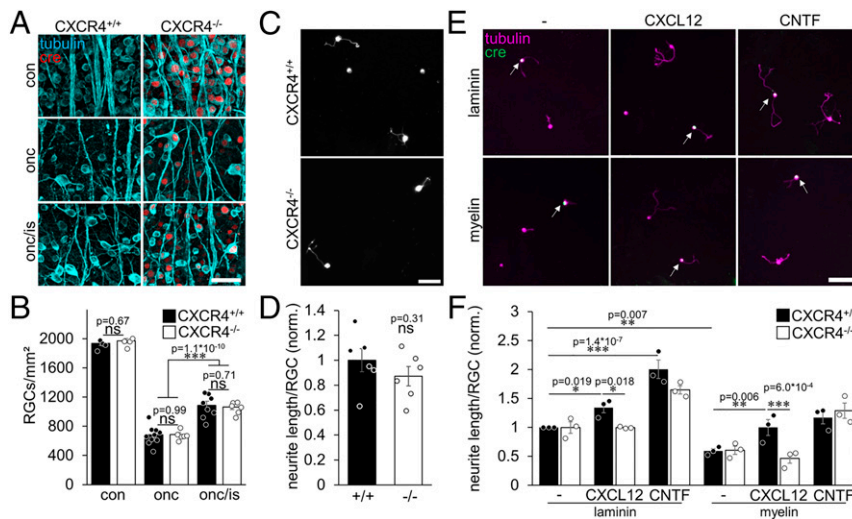
Conditional CXCR4 Knockout Affects Neither the Survival nor the Regenerative State of RGCs. To study the mechanism underlying the unexpected regeneration-promoting effect, we next tested whether RGC-specific CXCR4 depletion affects the survival or the intrinsic regenerative state of RGCs. Numbers of surviving RGCs were similarly reduced after ONC and partially rescued after neuroprotective IS independently of the CXCR4$^{-/-}$ in RGCs (Fig. 3 *A* and *B*). Also, adult CXCR4$^{+/+}$ and CXCR4$^{-/-}$ RGCs cultured either in the absence or presence of neuroprotective CNTF for 7 d (35) showed a similar decline in the number of surviving RGCs and a similar neuroprotective effect of CNTF (*SI Appendix*, Fig. S2 *A* and *B*). Moreover, adding recombinant CXCL12 to these cultures did not affect RGC survival either (*SI Appendix*, Fig. S2 *A* and *B*). Thus, CXCL12/CXCR4 signaling seemed irrelevant for RGC neuroprotection.

To evaluate whether the absence of CXCR4 affects the IS-mediated transformation of RGCs into a regenerative state, we analyzed the spontaneous neurite outgrowth of in vivo–stimulated RGCs in cell culture as described before (12, 13). To this end, mice received ONC/IS 5 d before the isolation of retinae and cell culture preparation. However, quantification of spontaneous neurite growth

revealed no measurable differences between CXCR4$^{-/-}$ and CXCR4$^{+/+}$ RGCs (Fig. 3 *C* and *D* and *SI Appendix*, Fig. S2*C*).

Conditional CXCR4 Knockout Abrogates Disinhibitory Effects of CXCL12. CXCR4's cognate ligand, CXCL12, is disinhibitory and moderately promotes neurite growth of rat RGCs on inhibitory myelin (18). To test whether the chemokine has a similar effect on mouse RGCs and whether this effect is CXCR4 dependent, we plated CXCR4$^{-/-}$ or CXCR4$^{+/+}$ RGCs either on laminin or myelin as described previously (9, 15). Additionally, half of the cultures were treated with CNTF to stimulate neurite outgrowth (9). As expected, CNTF enhanced neurite growth of RGCs on laminin, and myelin significantly compromised it (Fig. 3 *E* and *F*). Despite the growth-promoting effect of CNTF, myelin was still inhibitory (Fig. 3 *E* and *F* and *SI Appendix*, Fig. S2*D*), and these effects were similar in CXCR4$^{-/-}$ or CXCR4$^{+/+}$ RGCs (Fig. 3 *E* and *F* and *SI Appendix*, Fig. S2*D*). CXCL12 treatment of CXCR4$^{+/+}$ RGCs on laminin slightly increased neurite growth and overcame myelin inhibition (Fig. 3 *E* and *F* and *SI Appendix*, Fig. S2*D*). However, both effects were entirely abrogated by the CXCR4$^{-/-}$ in RGCs (Fig. 3 *E* and *F* and *SI Appendix*, Fig. S2*D*). Thus, although CXCR4 expression is irrelevant for neurite growth on laminin or myelin in the absence of CXCL12, it is required for the growth-promoting and disinhibitory effects of CXCL12.

Conditional CXCR4 Knockout Abolishes Chemoattractive Effects of CXCL12. Treatments overcoming myelin inhibition can facilitate optic nerve regeneration (14–16). Nevertheless, in an inhibitory environment such as the optic nerve's injury site, local accumulation of disinhibitory molecules may act chemoattractively toward axonal growth cones by favoring them to grow in the disinhibitory microenvironment. Therefore, disinhibitory CXCL12 at the optic nerve lesion site may restrain regenerating axons, preventing them

Hilla et al.
CXCR4/CXCL12-mediated entrapment of axons at the injury site compromises optic nerve regeneration

PNAS | 3 of 11
https://doi.org/10.1073/pnas.2016409118

Fig. 3. CXCR4$^{-/-}$ does not affect neuroprotection or the intrinsic regenerative state. (*A*) Confocal images of whole mounted retinae showing βIII-tubulin–positive RGC somata and their axons (tubulin, cyan). Immunohistological staining against Cre-HA identifies RGCs with a CXCR4 knockout (cre, red). Compared to untreated retinae (con), an optic nerve crush (onc) reduced the number of RGCs. In contrast, additional inflammatory stimulation (onc/is) was similarly neuroprotective for both CXCR4$^{-/-}$ and CXCR4$^{+/+}$ 14 d after injury. (Scale bar, 50 μm.) (*B*) Quantification of RGCs per square millimeter of groups, as described in *A*, showed no differences between knockouts and respective controls for either condition. Bars represent means ± SEM for $n = 4$ to 10 retinae per experimental group; dots represent single values per animal. Treatment effect: ****P* < 0.001, ns: nonsignificant by two-way ANOVA with Holm-Šídák post hoc test. (*C*) Photographs of dissociated RGCs from mice with RGC-specific CXCR4 knockout (CXCR4$^{-/-}$) and respective controls (CXCR4$^{+/+}$) that received ONC/IS 5 d before cell-culture preparation to increase their regenerative state. βIII-tubulin–positive RGCs extended neurites after cultivation for 24 h. (Scale bar, 50 μm.) (*D*) Quantification of neurite length per RGC showed no significant difference between CXCR4$^{-/-}$ and CXCR4$^{+/+}$. Values were normalized to the control group, with an average neurite length of 1.31 μm per RGC. Bars represent means ± SEM for $n = 6$ independent experiments; dots represent single values of experiments. Treatment effect: ns: nonsignificant by Student's *t* test. (*E*) Mixed cultures of CXCR4$^{+/+}$ and CXCR4$^{-/-}$ RGCs (cre; green, white arrows) grown on laminin or inhibitory myelin for 4 d with either vehicle, CXCL12, or CNTF as indicated. (Scale bar, 50 μm.) (*F*) Quantification of normalized neurite length per RGC from experimental groups displayed in *E*. CXCL12 or CNTF significantly elevated neurite growth of CXCR4$^{+/+}$ RGCs. Myelin reduced neurite growth. This inhibitory effect was overcome in the presence of CXCL12 and abolished by the CXCR4$^{-/-}$. Values were normalized to controls on laminin with an average neurite length of 10.71 μm per RGC. Bars represent means ± SEM for $n = 3$ independent experiments; dots represent single values of experiments. Treatment effects as indicated: **P* < 0.05, ***P* < 0.01, ****P* < 0.001, ns: nonsignificant by two-way ANOVA with Holm-Šídák post hoc test.

from growing distally. To test whether CXCL12 acts chemo-attractively, we developed an in vitro assay (*SI Appendix*, Fig. S3 *A–C*) in which in vivo–primed RGCs were plated on either laminin or CNS myelin. Culture inserts with CXCL12-secreting HEK293 cells were positioned in the center of each culture plate. The biological activity of secreted CXCL12 was verified before by testing the internalization of the CXCR4 protein in the presence of CXCL12 supernatant (*SI Appendix*, Fig. S3D) (24, 36). Cultures with CXCR4-positive RGCs (Fig. 4*A*) on growth-permissive laminin showed no measurable effect on neurites, while myelin-treated cultures showed significantly more regenerated neurites oriented toward the disinhibitory CXCL12 source (Fig. 4 *A–C*), indicating a chemoattractive effect on an inhibitory substrate. While AAV-GFP–transduced CXCR4$^{+/+}$ RGCs showed a similar attractive response, this effect was abolished in AAV-Cre–treated CXCR4$^{-/-}$ RGCs (Fig. 4 *A–C*). Thus, CXCL12 attracts neurites of mature RGCs CXCR4-dependently in an inhibitory environment.

Conditional CXCR4 Knockout Reduces U-Turns of Regenerating Axons in the Optic Nerve. Since the beneficial effect of CXCR4$^{-/-}$ on nerve regeneration could not be linked to neuroprotection or growth stimulation and CXCL12 was chemoattractive toward axons, we tested the hypothesis that CXCL12/CXCR4-mediated attraction around the lesion site affects the growth direction and prevents axons from growing distally in the nerve. To this end, we again used mice with CXCR4$^{-/-}$ or CXCR4$^{+/+}$ RGCs and analyzed regenerated axons using wholemount microscopy in cleared optic nerves 7 d after ONC/IS. At this early time point, a substantial number of anterogradely labeled axons had already grown short distances beyond the injury site (Fig. 4 *D–F*). Analysis of CXCR4$^{+/+}$ animals revealed that some axons regenerated relatively straight

along the optic nerve's longitudinal axis. However, a significant number grew aberrantly, with some axons making even U-turns back toward the lesion site (Fig. 4 *D* and *E*). In contrast, axons in animals with CXCR4$^{-/-}$ RGCs were significantly straighter and showed fewer U-turns (Fig. 4 *D* and *E*), resulting in an overall increased axon regeneration (Fig. 4*F*), suggesting a CXCR4-dependent attraction of growth-stimulated axons to the injury site.

RGCs Express CXCL12. Because CXCL12 was attractive toward RGC neurites (Fig. 4 *B* and *C*), we reasoned that cells at the lesion site could express and release this chemokine and generate a gradient. The detection of low but active levels of CXCL12 protein is challenging, as it is usually rapidly secreted and, after binding to its receptor, internalized. Therefore, we first tested whether CXCL12 mRNA expression is changed in retinae and optic nerves after ONC or ONC/IS (*SI Appendix*, Fig. S4 *A–C*). Optic nerves were divided into a proximal segment containing the crush site and a distal segment (*SI Appendix*, Fig. S4B). As determined by real-time PCR, CXCL12 expression in retinae or optic nerves was not significantly altered under naïve/undamaged or injured conditions (ONC or ONC/IS) (*SI Appendix*, Fig. S4 *A–C*), suggesting that neither resident cells nor infiltrating cells in the optic nerve caused significant up-regulation of CXCL12 expression. Nevertheless, to test whether resident cells in the optic nerve known to express low levels of CXCL12, such as microglia (27, 28) or astrocytes (27, 29), may be responsible for chemoattraction to the lesion site, we either depleted microglia or generated a transgenic mouse in which CXCL12 is specifically depleted in astrocytes upon tamoxifen injection (37). However, neither the complete depletion of microglia in the nerve (38), nor astrocytic CXCL12 knockout affected optic nerve regeneration (*SI Appendix*, Fig. S4 *C* and *D*). We then tested
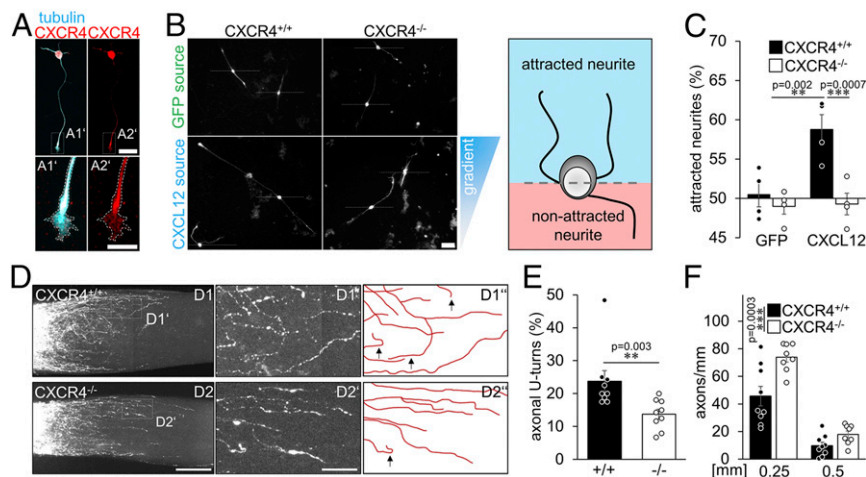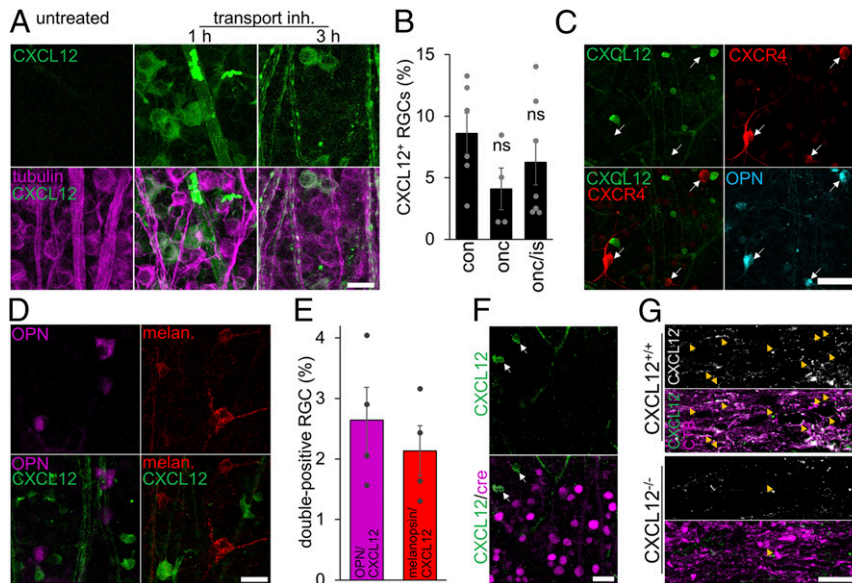
Fig. 4. CXCR4$^{-/-}$ overcomes inhibitory chemoattraction in the injured optic nerve. (*A*) CXCR4 staining (red) of regenerating βIII-tubulin–positive RGCs (cyan) after 4 d in culture. CXCR4 was detected in the soma and growth cones of neurites (magnification in A1′ & A2′). (Scale bar, 25 μm [overview] and 10 μm [magnifications].) (*B*) Cultured βIII-tubulin–positive RGCs with extending neurites exposed to either CXCL12-expressing (CXCL12 source) and -releasing HEK293 cells or GFP-expressing controls (GFP source). The triangle at the right indicates the CXCL12 concentration gradient with high concentrations at the top (blue) and low concentrations at the bottom (white). Dashed lines indicate the exclusion criterion: outgrowing neurites were counted as growing toward the source (neurite tip above the dashed line) or growing away from it. A schematic drawing highlights the criteria for analysis (s. also *SI Appendix*, Fig. S3 *A–C*). (Scale bar, 50 μm.) (*C*) Percentage of neurites of CXCR4$^{+/+}$ and CXCR4$^{-/-}$ RGCs growing toward the CXCL12 or control (GFP) source. While in the absence of a CXCL12 source, CXCR4$^{+/+}$ and CXCR4$^{-/-}$ RGCs fail to prefer a certain direction; more CXCR4$^{+/+}$ RGCs grow neurites into the direction of the CXCL12 source. This effect is completely abolished in CXCR4$^{-/-}$ RGCs. Bars represent means ± SEM for n = 4 independent experiments with 3 analyzed wells each, and dots represent single values per group (quantified neurites: GFP: CXCR4$^{+/+}$: 655, CXCR4$^{-/-}$: 280; CXCL12: CXCR4$^{+/+}$: 491, CXCR4$^{-/-}$: 284). Treatment effect: **$P < 0.01$, ***$P < 0.001$ by one-way ANOVA with Holm-Šídák post hoc test. (*D*) Confocal images of cleared optic nerves from CXCR4 knockouts (CXCR4$^{-/-}$) or respective controls (CXCR4$^{+/+}$) with CTB-labeled regenerating axons 7 d after crush and additional inflammataory stimulation. D1′ and D2′ show magnifications indicated in the overviews. D1″ and D2″ highlight the axonal trajectories and appearing U-turns (black arrows). Images were merged. (Scale bars, 75 μm [overview] and 25 μm [magnification].) (*E*) Quantification of the percentage of axons with U-turns from the 20 longest regenerating ones per optic nerve of experimental groups described in *D*. CXCR4$^{-/-}$ ($^{-/-}$) significantly reduces the numbers of U-turns compared to controls ($^{+/+}$). Bars represent means ± SEM for n = 9 animals per group; dots represent single values per group. Treatment effect: **$P < 0.01$ by χ^2 test. (*F*) Quantification of regenerating axons extending indicated distances beyond the injury site from groups described in *D*. Upon CXCR4 depletion, more axons crossed the lesion site and regenerated into the distal optic nerve 7 d after ONC/IS compared to controls. Values represent means ± SEM for 8–9 mice per experimental group (CXCR4$^{+/+}$: n = 9; CXCR4$^{-/-}$: n = 8). Dots represent single values of each animal. Treatment effects: ***$P < 0.001$; ns: nonsignificant by two-way ANOVA with Holm-Šídák post hoc test.

whether CXCL12 protein could be released from injured axons at the lesion site. This idea was driven by previously published data showing CXCL12 mRNA expression in a subpopulation of postnatal RGCs (39). Because the rapid transport and secretion of endogenous CXCL12 do not allow reliable detection of the chemokine in neurons, we intravitreally injected a reversible protein transport inhibitor 1 or 3 h before retinal wholemount preparation. As this inhibitor causes a reversible disintegration of the Golgi apparatus (40, 41), the secretory pathway is halted, and the protein accumulates in the cell body. Retinae exposed to the inhibitor for 1 h showed clear signals in about 8% of uninjured RGCs and RGCs 14 d after axotomy (Fig. 5 *A* and *B*). When examined at 3 h after injection, pronounced vesicular signals were additionally detectable in retinal axons (Fig. 5*A*), implying that the chemokine's axonal transport had started again (40, 41). Interestingly, CXCL12-positive RGCs were negative for CXCR4, and only very few were positive for OPN or melanopsin (Fig. 5 *C–E*), suggesting that neurons expressing the chemokine represent another subpopulation. The signal specificity was verified using CXCL12-floxed mice that had received an intravitreal AAV2-Cre injection. Accordingly, RGCs with the CXCL12 knockout showed no CXCL12 signal (Fig. 5*F*). In addition, immunohistochemical staining of longitudinal optic nerve sections from animals 4 d after ONC/IS revealed CXCL12-positive axons in the proximal optic nerve near the lesion site (Fig. 5*G*). In contrast, only very few remaining axons with CXCL12-positive puncta were found in AAV-Cre–treated CXCL12-floxed mice, representing the few nontransduced and, hence, remaining CXCL12$^{+/+}$ RGCs (Fig. 5*G*). We also immunocytochemically detected endogenous CXCL12 in cultured adult

RGCs as puncta throughout their somata and extended neurites (Fig. 6*A*), implying its vesicular transport as described previously (42).

Viral overexpression of exogenous CXCL12 in RGCs further increased the intensity and number of CXCL12-positive puncta (Fig. 6*A*). To verify the axonal transport and secretion of CXCL12 at axonal tips, we cultured adult sensory neurons from dorsal root ganglia (DRG) in two-compartment chambers. In contrast to RGCs, these neurons can be cultured for several days allowing axon growth through the microchannels. A CXCL12 baculovirus or respective GFP baculovirus was added in the somal chamber to exogenously express CXCL12 in these neurons (Fig. 6 *B* and *C*). Moreover, the transport inhibitor was added to some of the somal chambers, and 2 d later, media from the axonal compartments were collected. As determined by enzyme-linked immunosorbent assay (ELISA), secreted CXCL12 was identified in axonal compartments of CXCL12-transduced sensory neurons (Fig. 6*D*). In contrast, cultures treated with the transport inhibitor showed almost no CXCL12 in the axonal chambers' medium (Fig. 6*D*). To verify the axonal transport and accumulation of the chemokine at the lesion site, we transduced RGCs with an AAV2 carrying the construct of an HA-tagged CXCL12 distinguishable from endogenous protein (Fig. 6*E*). To allow us to identify single axon tips at the lesion site, we injected less virus into the vitreous to reduce the transduction rate to about 30% (Fig. 6*F*). Optic nerves were prepared for immunohistochemical analysis 5 d after ONC. HA staining was found in GFP-positive somata/transduced neurons (Fig. 6 *E* and *F*) and single axons in the proximal nerve segment, while in controls (AAV-GFP), the HA signal was absent (Fig. 6*F*). However, HA staining was not restricted anymore to GFP-positive

Hilla et al.
CXCR4/CXCL12-mediated entrapment of axons at the injury site compromises optic nerve regeneration

PNAS | 5 of 11
https://doi.org/10.1073/pnas.2016409118

Fig. 5. CXCL12 is expressed in a subset of RGCs. (*A*) Confocal images of retinal wholemounts. Intravitreal injection of a transport inhibitor mixture 1 h before tissue isolation reveals accumulated CXCL12 protein (green) in RGC somata and their axons 3 h after treatment (tubulin, magenta). (Scale bar, 20 μm.) (*B*) Quantification of the percentage of CXCL12-expressing RGCs in untreated retinae (con) and 2 wk after optic nerve crush (onc) or ONC and additional inflammatory stimulation (onc/is) show similar numbers of CXCL12-positive RGCs. All eyes received intravitreal injection of the transport inhibitor mixture before tissue harvest. Bars represent means ± SEM for n = 4 to 7 retinae per group; dots represent values of individual retina. Treatment effects: ns = nonsignificant by one-way ANOVA. (*C*) Representative images of wholemounted retina with CXCL12-positive RGCs (green, 1 h after transport inhibitor treatment), which all do not express CXCR4 (red, white arrow) and are not α-RGCs (OPN, cyan). (Scale bar, 50 μm.) (*D*) Representative images of wholemounted retinae with CXCL12-positive RGCs (green, 1 h after secretion inhibitor treatment) that do not overlap with the α-RGC subtype (OPN, magenta) or the ipRGC subtype (melanopsin, red). (Scale bar, 25 μm.) (*E*) Quantification of OPN/CXCL12 and melanopsin/CXCL12 double-positive RGCs. Bars represent means ± SEM for n = 4 retinae per group; dots represent single values. (*F*) CXCL12$^{-/-}$ retina that received intravitreal injection of the secretion inhibitor 1 h before isolation show no CXCL12 staining for transduced RGCs (cre, magenta). Very few nontransduced cells still express CXCL12 (green, white arrows). (Scale bar, 25 μm.) (*G*) Longitudinal optic nerve sections show CXCL12-positive (white or green) CTB-labeled axons (magenta, arrow) in control mice (CXCL12$^{+/+}$) 4 d after ONC/IS. In contrast, only a few axons showed CXCL12-positive puncta in AAV-Cre–treated CXCL12-floxed mice, which most likely display nontransduced and, hence, CXCL12$^{+/+}$ RGCs. (Scale bar, 25 μm.)

axonal tips at the lesion site and appeared somewhat blurry, suggesting its release and accumulation in the environment of axonal tips (Fig. 6*F*).

Conditional CXCL12 Knockout Mimics Conditional CXCR4 Knockout Effects. To prove that RGC-derived CXCL12 is involved in retaining CXCR4-positive axons at the lesion site, we intravitreally injected either AAV-Cre or AAV-GFP into CXCL12-floxed mice, resulting in either CXCL12$^{-/-}$ or CXCL12$^{+/+}$ RGCs. After a period of 3 wk, mice were subjected to ONC/IS as described before, and optic nerve regeneration was determined after another 3 wk. Strikingly, the knockout of CXCL12 in RGCs led to a similar potentiating effect on regeneration as observed after RGC-specific CXCR4 depletion (Fig. 7 *A* and *B*). Just as with the conditional CXCR4 knockout, the ligand's knockout did not affect RGC survival after ONC/IS (Fig. 7 *C* and *D*). Additionally, we analyzed axonal trajectories 7 d after ONC/IS. Also, CXCL12$^{-/-}$ in RGCs significantly reduced the number of axons with U-turns as RGC-specific CXCR4 depletion, resulting in an overall increased axon regeneration (Figs. 7 *E–G* and 4 *D–F*).
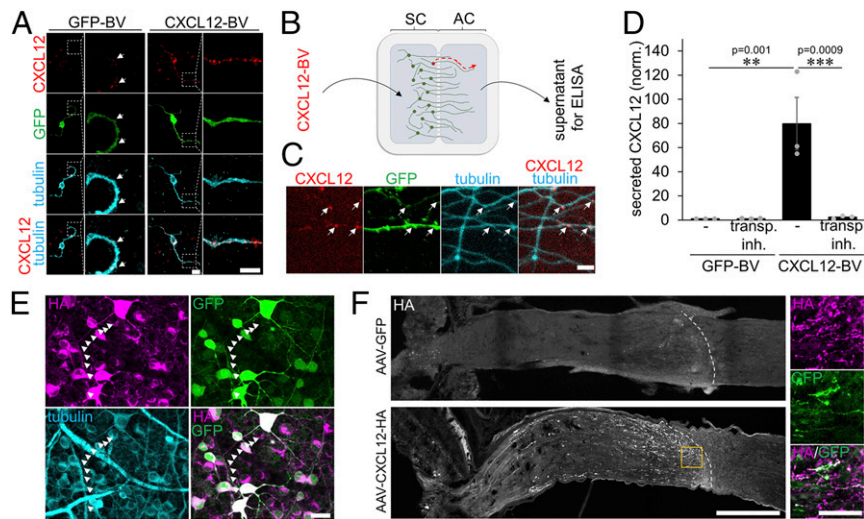
Discussion

Using adult mice, the current study shows that 1) a proportion of RGCs express CXCL12 protein, 2) CXCL12 is axonally transported and released at axonal tips, 3) CXCR4 is expressed in α-RGCs and their axons, 4) CXCL12 is chemoattractive to axons in an inhibitory environment, and 5) neuronal knockout or knockdown of either CXCL12 or CXCR4 reduces entrapment of axons and potentiates IS-stimulated axon growth in the adult optic nerve. The regeneration achieved by RGC-specific CXCR4 or CXCL12 knockouts + IS was stronger than the effects of PTEN knockout and

similar to that of hIL-6 treatment, one of the strongest measures promoting regeneration (43–45). Together, these data suggest that RGC-derived CXCL12 is released at the injury site and averts axon extension of CXCR4-expressing RGCs in the inhibitory distal nerve by chemoattraction. Thus, intervention with CXCR4/CXCL12 signaling may open a clinically applicable approach to facilitate axonal regeneration in the injured CNS.

Various cell types of the developing and adult CNS express CXCL12 and its receptor CXCR4, including endothelial and glial cells and neurons (18, 19, 27–29, 46, 47). In some brain regions, CXCL12 and CXCR4 are coexpressed even in the same cells, suggesting that they constitute a functional ligand/receptor system in specific neuronal pathways (20, 27, 28, 46, 47). Thus, CXCL12 protein might be secreted at the injury site by different cell types, such as microglia (27, 28) or astrocytes (27, 29). However, ONC did not increase CXCL12 gene expression in the optic nerve. Furthermore, neither complete depletion of microglia (38) nor the knockout of CXCL12 in astrocytes (*SI Appendix*, Fig. S4 *D* and *E*) mimicked the effects of CXCR4$^{-/-}$. Although we cannot exclude any contribution of glial-derived CXCL12, these cells could not be the primary chemokine source causing axonal entrapment at the lesion site.

A previous study recently reported mRNA expression of CXCR4 and CXCL12, each in different subpopulations of postnatal RGCs (39). Similarly, the current study shows the expression of CXCL12 protein in RGCs of adult mice. The chemokine was detectable in ∼8% of RGCs and their axons in the optic nerve, where it showed a vesicular staining pattern indicating its axonal transport. To confirm the anterograde transport of the secretable chemokine in RGCs, we intravitreally applied a reversible transportation inhibitor to transiently block its release from the endoplasmic reticulum (40, 41).

Hilla et al.
CXCR4/CXCL12-mediated entrapment of axons at the injury site compromises optic nerve regeneration

Fig. 6. Axonal transport and release of CXCL12 in the optic nerve. (*A*) Confocal image of cultured adult RGCs transduced with either a GFP- (GFP-BV) or a CXCL12/GFP-coexpressing BV (CXCL12-BV). CXCL12-positive puncta (red) are distributed throughout RGC somata and neurites (tubulin, cyan) of GFP-BV–treated RGCs. The number and signal of puncta increased in CXCL12-BV–treated, and therefore overexpressing, RGCs. GFP expression (green) indicates successful transduction by respective BVs. Dotted areas are magnified to highlight CXCL12 puncta. (Scale bars, 10 μm [overview] and 5 μm [magnification].) (*B*) Adult sensory dorsal root ganglion neurons were cultured in microfluidic two-compartment chambers. Cell bodies in the soma compartment were transduced with a BV coexpressing CXCL12/GFP (CXCL12-BV) or with a GFP-expressing control virus. CXCL12 was transported within axons and released at axon terminals in the axonal compartment (AC). AC supernatants were collected and used for an ELISA. (*C*) Confocal microscopic images of axons after CXCL12-BV treatment as described in *B* show CXCL12-positive puncta (red) in transduced (GFP, green) axons (tubulin, cyan). (Scale bar, 10 μm.) (*D*) ELISA of axon compartment supernatants after BV-mediated CXCL12 expression (CXCL12-BV) or respective control (GFP-BV). Compartments received new media either with or without a transport inhibitor (transp. inh.) 3 d after culture preparation to inhibit protein transport and secretion or respective control (-). After 48 h, media were collected and analyzed by ELISA. Columns show the amount of secreted CXCL12 (normalized to GFP-BV, -), dots the individual experiments ($n = 3$). Treatment effects: **$P < 0.01$, ***$P < 0.001$ by two-way ANOVA with Holm-Šídák post hoc test. (*E*) Confocal image of a retina 14 d after intravitreal injection of AAV2-CXCL12-HA shows transduced βIII-tubulin–positive RGCs (cyan) as visualized by GFP expression (green). Transduced RGCs express HA-tagged CXCL12 (HA, magenta), which is also present in axons (white arrowheads). (Scale bar, 25 μm.) (*F*) Confocal image of an AAV-CXCL12-HA–injected mouse optic nerve shows HA-positive axons (white) that terminate at the lesion site (dotted white line) 5 d after optic nerve crush. Magnifications (orange rectangle) highlight the accumulation of secreted CXCL12-HA from GFP-positive axon terminals at the lesion site as verified by HA staining (magenta). In contrast, AAV-GFP–injected controls show no HA staining in the optic nerve. (Scale bars, 250 μm [overview] and 50 μm [magnifications].)

Consistently, an injection shortly before retina isolation markedly increased the intensity of CXCL12 staining in the neuronal cell bodies, indicating its accumulation there. In tissues collected at later time points, a pronounced CXCL12 staining was also found in retinal axons. These showed a typical granular staining pattern, most likely reflecting the restarted anterograde transport of vesicles containing the previously accumulated protein in the soma. To test whether CXCL12 can be released from injured axons, we cultured primary adult sensory neurons in two-compartment chambers separating axon terminals from the somata. Adult RGCs could not be used for this purpose due to their limited axon growth rate and limited survival time in culture. Although it cannot be entirely excluded that CXCL12 transport occurs differently in RGCs and DRG neurons, mechanisms are similar in both cell types. In accordance, immunohistochemical staining of cultivated RGCs or DRG showed CXCL12 localization in the neurites upon viral overexpression. These experiments showed that virally expressed CXCL12 is anterogradely transported and released from axonal terminals into the axonal chamber's medium. These findings were confirmed in vivo by the viral overexpression of exogenous, HA-tagged CXCL12, whose accumulation was detected at the lesion site. The results described above corroborate previous reports that CXCL12 is a secretory chemokine (25, 42, 46, 48). Moreover, the findings that both CXCL12 and CXCR4 knockouts in RGCs similarly reduced aberrant growth and enabled long-distance regeneration also imply its release and interaction with the CXCR4-positive axons in vivo. Depletion of CXCR4 or CXCL12 did not impair neuroprotection, and CXCR4 knockout did not measurably reduce the regenerative state of RGCs. In contrast, it enhanced IS-induced regeneration. Thus, other cells, such as leukocytes, potentially attracted by CXCL12 and involved in IS-mediated effects

(7, 49, 50) are unlikely to play a significant role in the long-distance regeneration enabled by CXCR4$^{-/-}$. The physiological role of CXCL12 in the adult visual system, such as neuromodulation in other tissues (47, 51), remains to be elucidated. However, its adverse effect after ONC may be derived from its essential role during development, during which CXCL12/CXCR4 signaling is relevant for neurogenesis (52, 53), axonal guidance (20, 32), and axonal outgrowth (54). Consistently, in zebrafish, ectopic expression of CXCL12 near the optic nerve as well as morpholino-mediated CXCL12 and CXCR4 knockdown caused aberrant growth of RGC axons (20). While CXCL12 does not mediate disinhibition toward chondroitin sulfate proteoglycans such as neurocan (18), it overcomes inhibition of CNS myelin (32) and repellant guidance molecules such as Slit in retinal explant cultures, thereby affecting axonal growth (32). Accordingly, the current study confirmed the disinhibitory effect of CXCL12 toward myelin and showed that it is mediated via CXCR4. Moreover, CXCL12 also attracted neurites on inhibitory CNS myelin, suggesting that gradually increasing concentrations of the disinhibitory chemokine affects the orientation of regrowing axons in an inhibitory environment. The proposed attraction by disinhibition does not contradict the concept of inhibitory molecules compromising regeneration. Instead, it adds another aspect: disinhibitory molecules in the proximal nerve segment, such as CXCL12, become attractive in an inhibitory environment. It is currently unknown how long CXCL12 remains biologically active once it is released. However, proteoglycan sidechains in the glial scar reportedly bind CXCL12 and delay its degradation, suggesting an extended chemokine availability toward CXCR4-positive axons (48, 55). Furthermore, the amount of CXCL12-producing RGCs drops only slightly 2 wk after optic nerve injury, providing further evidence for sustained CXCL12 secretion. This is of particular relevance as
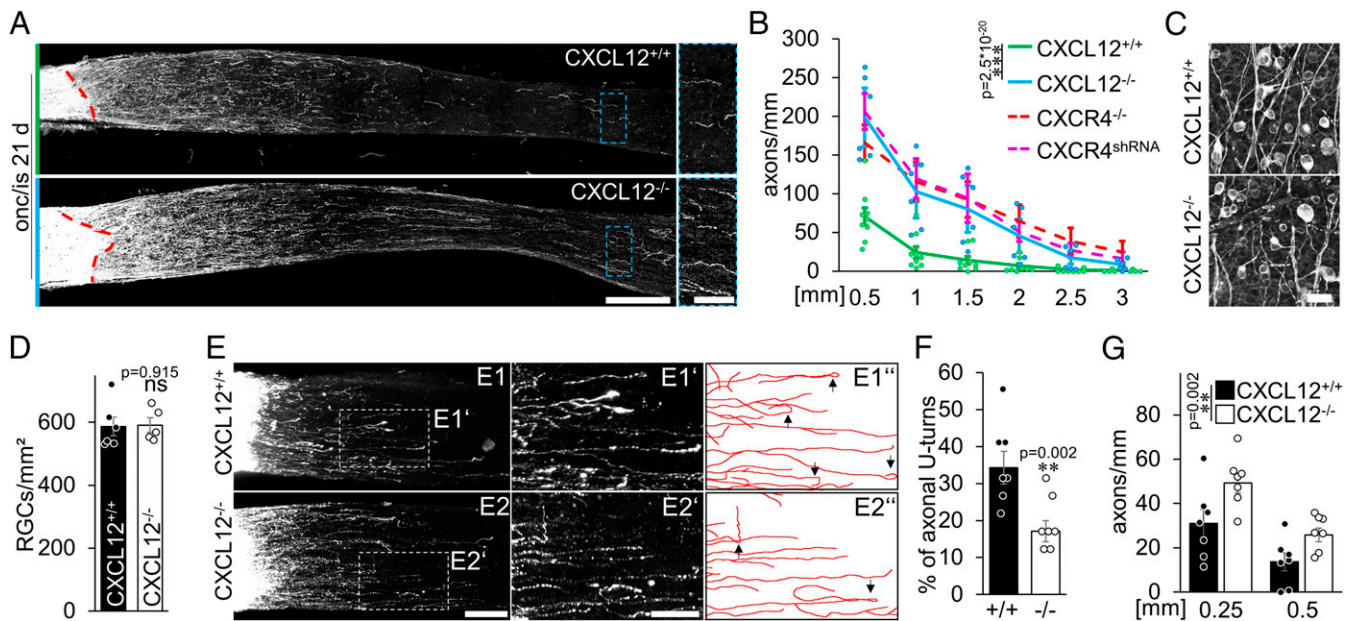
Fig. 7. CXCL12$^{-/-}$ enables long-distance regeneration. (*A*) Longitudinal optic nerve sections with CTB-labeled regenerating axons 21 d after optic nerve crush and additional inflammatory stimulation (onc/is). Nerves were isolated from mice that received a conditional CXCL12 knockout in RGCs (CXCL12$^{-/-}$) or from respective controls (CXCL12$^{+/+}$). The dashed red line indicates the injury site. The dashed blue boxes indicate the magnified area on the right. (Scale bars, 200 μm [overview] and 50 μm [magnification].) (*B*) Quantification of regenerating axons extending 0.5, 1, 1.5, 2, 2.5, and 3 mm beyond the injury site on sections as described in *A*. Results from the CXCR4 knockout (CXCR4$^{-/-}$) and knockdown (CXCR4^{shRNA}) shown in Fig. 2 (dashed lines) were included for comparison. Optic nerve regeneration of CXCL12$^{-/-}$ was increased to a similar extent as in CXCR4$^{-/-}$ or CXCR4^{shRNA} groups. Values represent means ± SEM for 6 to 9 mice per experimental group and 5 sections per animal (CXCL12$^{+/+}$: $n = 9$; CXCL12$^{-/-}$: $n = 6$). Treatment effect: ***$P < 0.001$ by two-way ANOVA with Holm-Šídák post hoc test. (*C*) Confocal image of wholemounted retinae showing similar numbers of βIII-tubulin–positive RGCs for CXCL12$^{-/-}$ and respective CXCL12$^{+/+}$ controls 21 d after ONC/IS. (Scale bar, 25 μm.) (*D*) Quantification of RGC densities per square millimeter of groups as described in *C*. Bars represent means ± SEM for $n = 5$ to 6 animals per group; dots represent single values. Treatment effect: ns: nonsignificant by Student's *t* test. (*E*) Confocal images of optic nerves from mice with CXCL12$^{-/-}$ or CXCL12$^{+/+}$ showing CTB-labeled regenerating axons 7 d after ONC/IS. E1′ and E2′ show magnifications indicated by dashed boxes in the overviews, while E1″ and E2″ highlight the axonal trajectories and appearing U-turns (black arrows). (Scale bars, 100 μm [overview] and 50 μm [magnification].) (*F*) Proportion of axonal U-turns from the 20 longest regenerating axons per optic nerve of experimental groups as described in *E*. CXCL12$^{-/-}$ reduces axonal U-turns compared to controls CXCL12$^{+/+}$. Bars represent means ± SEM for $n = 7$ animals per group; dots represent single values. Treatment effect: **$P < 0.01$ by χ^2 test. (*G*) Quantification of regenerating axons extending indicated distances beyond the injury site from groups described in *E*. Upon CXCL12 depletion, more axons crossed the lesion site and regenerated into the distal optic nerve 7 d after ONC/IS compared to controls. Values represent means ± SEM for seven mice per experimental group (CXCL12$^{+/+}$: $n = 7$; CXCL12$^{-/-}$: $n = 7$). Dots represent single values of each animal. Treatment effects: **$P < 0.01$ by two-way ANOVA with Holm-Šídák post hoc test.

almost all CXCR4-expressing neurons are α-RGCs. This subpopulation is highly resilient to axotomy-induced RGC degeneration and represents the main surviving subpopulation over several weeks after axotomy (33). Moreover, this subpopulation mainly extends axons in the distal optic nerve after crush injury and PTEN knockout (33). As CXCR4-expressing neurons are particularly sensitive toward secreted chemoattractive CXCL12, the chemokine release likely favors tortuous axon growth at the lesion site reported previously by others (56) and consequently limits axon extension into the distal, more inhibitory segment of the injured nerve (56). Accordingly, about 25% of the longest regenerating axons showed aberrant growth (U-turns) early after injury, while CXCR4$^{-/-}$ or CXCL12$^{-/-}$ in RGCs approximately halved this number. Nevertheless, RGC-specific CXCR4 and CXCL12 depletion did not abolish all aberrant growth, potentially because our virally induced knockouts reached only 80 to 90% of all RGCs or because additional attractive or repulsive molecules may also contribute to aberrant growth as shown during development (57). The CXCR4/CXCL12-dependent mechanism likely entraps most axons in the lesion site, and the U-turns indicate that even some regenerating axons were attracted back. Therefore, it is likely that RGC-specific CXCR4 and CXCL12 depletion prevent U-turns and release the captured axons. However, because of the high axonal density in the lesion site, it is impossible to trace individual trajectories. Although our data strongly suggest that CXCR4$^{-/-}$-promoted regeneration was caused by CXCL12-mediated

attraction, we cannot entirely exclude the contribution of additional mechanisms entrapping axons at the injury site, such as forming synaptic-like contacts between growth cones or NG2 glia, as described in the lesioned dorsal columns and at the dorsal root entry zone after root crush (58). Moreover, it is currently unknown whether CXCL12/CXCR4 interactions between axons are also occurring along the axon shafts in the proximal nerve stump and cause fasciculation, which could also prevent axons from growing beyond the lesion site.

The current study's findings that CXCL12/CXCR4-mediated signaling compromises axon regeneration may have implications for new strategies for CNS repair. Besides the CXCR4 and CXCL12 knockdown, identifying the downstream signaling pathways relevant for the CXCR4/CXCL12-mediated attraction/retention may help develop pharmacological inhibitory compounds. For example, one candidate could be the CXCR4 inhibitor AMD3100 (18, 32, 59), whose application needs to be tested in the future. Another approach that can be derived from this is the use of CXCL12 to guide axons beyond the injury site. In this context, the ectopic expression of CXCL12 in the distal optic nerve may help to attract axons beyond the lesion site or even guide them to their appropriate targets. The latter aspect deserves particular attention because various approaches allowing axon regeneration beyond the optic chiasm have reported misguidance. Some regenerating fibers grow into the wrong optic tract or even into the contralateral optic nerve (13, 60, 61). It also needs to be tested whether inhibition of CXCR4/CXCL12-mediated

axonal retention can also promote axon regeneration in other CNS lesion models such as the spinal cord.

In conclusion, the finding that CXCR4/CXCL12 signaling inhibits regeneration by attracting and hence containing regenerating axons at the optic nerve's injury site provides a so far unknown mechanism that contributes to regenerative failure. It therefore opens new possibilities for therapeutic strategies. Next to viral knockdown in neurons, as presented here, pharmacologic approaches aiming to counteract CXCR4/CXCL12 signaling could be considered for testing in the future.

Materials and Methods

Animal Experiments and Surgical Procedures. All experimental procedures were approved by the local animal care committee (Landesamt für Natur-, Umwelt- und Verbraucherschutz, Recklinghausen) and conducted in compliance with federal and state guidelines for animal experiments in Germany. For the current study, we used 2- to 3-mo-old male and female Lewis rats or C57BL/6J, B6(FVB)-Cxcl12tm1.1Link/J (CXCL12-floxed), B6.129P2-Cxcr4tm2Yzo/J (CXCR4-floxed), and B6(FVB)-Cxcl12tm1.1Link/J TgN(hGFAP-CreERT2)GCTF-Fki (GFAP-CreER CXCL12-floxed) mice. All animals were housed for at least 10 d before starting experiments and maintained on a 12-h light/dark cycle with ad libitum access to food and water.

Animals were anesthetized by intraperitoneal injections of ketamine (100 mg/kg) and xylazine (10 mg/kg). ONC was performed 1 mm behind the eyeball using jeweler's forceps (Hermle) as described previously (8, 9). The crush's completeness was verified for each animal by the absence of spared axons in the optic chiasm (34). IS was induced by retrolental lens puncture by a glass capillary immediately after ONC to increase the regenerative capacity of injured RGCs (5). A period of 2 d before tissue isolation, regenerating axons were labeled by intravitreal injection of 2 μL Alexa Fluor 555-conjugated cholera toxin β subunit (0.5% CTB, in phophate buffered saline [PBS]; Molecular Probes).

Immunohistochemistry. Animals were anesthetized and intracardially perfused with ice-cold PBS followed by 4% paraformaldehyde (PFA) in PBS. Eyes and attached optic nerves were removed from connective tissue, postfixed overnight in 4% PFA/PBS at 4 °C, and subsequently transferred to 30% sucrose for at least 4 h. Tissues were embedded in the KP-cryo compound (Klinipath), cut longitudinally or in cross-sections (14 or 30 μm) on a CM3050 S cryostat (Leica Biosystems), thaw-mounted onto charged glass slides (Superfrost Plus, VWR), and stored at −20 °C until further use.

Retinal wholemounts were prepared as described elsewhere (62) and detailed in the *SI Appendix*.

To amplify the CXCR4 signal in untreated murine retinae, a Tyramide Signal Amplification Kit (ThermoFisher) was used according to the manufacturer's protocol. Immunohistochemical proof of CXCR4 knockout and knockdown, such as examination of colocalization with CXCL12, was performed in murine retinae 14 d after ONC.

Sections and wholemounts were coverslipped with Mowiol and analyzed using either fluorescent (Axio Observer.D1; Zeiss) or confocal laser scanning (LSM510; Zeiss, or SP8; Leica) microscopes.

Quantification of Regenerating Axons in the Optic Nerve. Axon regeneration of optic nerves 7 or 21 d after ONC or ONC/IS was quantified as described previously (13) and described in the *SI Appendix*.

U-Turn Analysis of Regenerated RGC Axons. After a period of 3 wk, the intravitreal application of AAV2-Cre or AAV2-GFP, CXCR4-or CXCL12-floxed mice were subjected to ONC/IS. The anterograde tracer CTB conjugated to Alexa Fluor 555 (Invitrogen) was intraocularly injected 5 d after the injury, and the tissue was harvested after another 2 d. Anesthetized animals were perfused as described previously; the optic nerves were carefully removed and postfixed overnight in 4% PFA (9). Tissue clearing was performed as described elsewhere (63) and detailed in the *SI Appendix*. Z-stacks of cleared optic nerve wholemounts were imaged using a confocal laser scanning microscope with a thickness of 1.038 μm per z-plane and an overlap of 32% between z-planes, resulting in 341 to 521 images per optic nerve. To accurately record the trajectories of individual axons, the z-stacks were visualized using the Vaa3D software. Because regenerating axons near the lesion site could not be accurately resolved, the 20 longest axons were tracked and analyzed, as they were clearly distinguishable from one another. Axonal tips that deviated more than 90° from the longitudinal axis of the optic nerve or

pointing toward the lesion site were counted as a U-turn (arrows in Figs. 4 *D* and 7 *E*). Experimental groups included seven to nine mice.

Verification of AAV-CXCR4^shRNA. HEK293 cells were transfected with either a control plasmid expressing GFP, a plasmid expressing CXCR4 together with GFP, or a combination of the CXCR4-expressing plasmid together with a plasmid containing the CXCR4^shRNA by Lipofectamine-2000 (ThermoFisher) according to the manufacturer's protocol. Cells have either been fixated in a 4% PFA solution for immunohistochemical staining as described above or collected and lysed for Western blot analysis.

Quantification in Retinal Wholemounts. Quantification of surviving RGCs in retinal wholemounts 14 d after ONC or ONC/IS was performed as described previously (62) and detailed in the *SI Appendix*.

To quantify the number of CXCR4-positive RGCs, confocal images of naïve and axotomized retinae were taken of each retinal quadrant. Only CXCR4-positive signals that clearly colocalized with βIII-tubulin staining were counted as CXCR4-positive RGCs or RGC axons. This number was then divided by the number of all tubulin-positive RGCs/RGC axons to assess the relative amount.

Analysis of CXCL12 Expression and Knockout in RGCs. To quantify the amount of CXCL12-positive RGCs in retinae 14 d after ONC or ONC/IS compared to respective untreated controls, mice received an intravitreal injection of 2 μL undiluted Protein Transport Inhibitor Mixture containing Brefeldin A and Monensin (eBioscience Protein Transport Inhibitor Mixture, 500X; Thermo-Fisher). This inhibitor prevents protein transport and secretion and thus causes an accumulation of proteins in the soma. After 1 or 3 h, retinal wholemounts have been prepared as described above and immunohistochemically stained against CXCL12 (1:250; R&D Systems; RRID: AB_2088149) and βIII-tubulin (1:1,000; BioLegend, RRID: AB_2313773). To quantify the number of CXCL12-positive RGCs, confocal images were taken, and the number of CXCL12-positive RGCs was divided by the number of all tubulin-positive RGCs. On average, 214 tubulin-positive RGCs were present per confocal image, and 4 images were acquired per retinal wholemount.

To verify the specificity of the CXCL12 knockout, CXCL12-floxed mice received an intravitreal injection of AAV2-Cre-HA or AAV2-GFP. After 3 wk, mice of either group received an intravitreal dose of undiluted Protein Transport Inhibitor Mixture, from which retinal wholemounts were prepared as described above. Retinal wholemounts were then immunohistochemically stained against HA (1:1,000, Sigma-Aldrich, RRID: AB_260070) to label RGCs transduced by AAV2-Cre-HA and against CXCL12 (1:250; R&D Systems; RRID: AB_2088149). To verify CXCL12 localization in RGC axons and the absence of the protein in respective CXCL12 knockouts, mice were subjected to ONC/IS, and axons anterogradely labeled by Alexa Fluor–conjugated CTB as described above. After 4 d, mice have been perfused, and the optic nerves have been embedded and cut into 30 μm–thick longitudinal cryo-sections as described above. Confocal images were acquired in the axotomized optic nerve proximal part using a confocal laser scanning microscope.

Dissociated Retinal Cell Cultures. The RGC-specific CXCR4 knockout was induced by intravitreal injection of AAV2-Cre-HA 3 wk before tissue isolation. To study the effect of different compounds on RGC neurite outgrowth (in vitro condition) or survival, we prepared retinal cultures as described previously (9, 10) and detailed in the *SI Appendix*.

Chemoattraction Assay. To investigate the sensitivity of RGC neurites toward CXCL12, we established a chemoattraction assay. To this end, ONC/IS-stimulated CXCR4^+/+ or CXCR4^−/− RGCs generated by intravitreal injection of AAV2-Cre-HA or AAV2-GFP in adult CXCR4-floxed mice were cultured together with a CXCL12 source or controls on poly-D-lysine/laminin/myelin coated 6-well plates (Nunc). Regarding the CXCL12 source, HEK293 cells were transfected by Lipofectamine-2000 (ThermoFisher) according to the manufacturer's protocol with either a CXCL12 expression vector or GFP vector. After 24 h, 3×10^5 cells were seeded into a cell culture insert containing a membrane with a pore size of 3 μm (Merck Millipore), allowing the chemokine release. The insert was then placed into the center of a well containing the dissociated RGCs to establish a CXCL12 gradient. The cell culture medium was carefully replaced every 24 h to maintain the gradient. After 3 d in culture, RGCs were fixed and subsequently stained for βIII-tubulin. Pictures of RGCs with extended neurites were taken under a fluorescent microscope (×200, Axio Observer D1, Zeiss), and neurites were analyzed for their orientation toward the cellular chemokine source (Fig. 4 *B* and *SI Appendix*, Fig. S3 *C*). To do so, a line perpendicular toward the cell culture insert divides the RGC into two virtual spaces. All neurite tips present in the space toward the insert are counted as attracted neurites (Fig. 4 *B* and *SI Appendix*,

Hilla et al.
CXCR4/CXCL12-mediated entrapment of axons at the injury site compromises optic nerve regeneration

PNAS | 9 of 11
https://doi.org/10.1073/pnas.2016409118

). The experiment was performed four times, with three wells per experiment analyzed.

DRG Neuron Two-Compartment Cultures. DRG neurons were harvested from adult mice as previously described (64). In brief, isolated DRG (T8-L5) were incubated in 0.25% trypsin/EDTA (GE Healthcare) and 0.3% collagenase Type IA (Sigma) dissolved in Dulbecco's modified Eagle medium (DMEM) (Invitrogen) at 37 °C and 5% CO_2 for 45 min and mechanically dissociated afterward. Cells were resuspended in DMEM containing B27-supplement (1:50, Invitrogen) and penicillin/streptomycin (500 U/mL; Merck Millipore), and seeded into the somal compartment of microfluidic two-compartment chambers (AXIS Axon Isolation Device, Millipore), mounted on poly-D-lysine (0.1 mg/mL, molecular weight 70,000 to 150,000 Da; Sigma) plus laminin-coated (20 μg/mL; Sigma) culture dishes according to the manufacturer's instructions. Neurons were cultured at 37 °C, 5% CO_2 and transduced with CXCL12-expressing baculoviruses (BV) or GFP-expressing control BV (65). Diffusion of particles or proteins through the microchannels into the axonal compartment was prevented by using a hydrostatic pressure due to two different volumes of medium with a resulting antagonistic microflow of liquid between the axonal and the somal chambers. After 24 h, the virus-containing medium was replaced with fresh culture medium (DMEM, 1:50 B27 supplement and 1:50 penicillin/streptomycin). After another 48 h, a time point where DRG axons already grew through the microchannels into the axon compartment, the medium was replaced again containing Protein Transport Inhibitor Mixture (1x, ThermoFisher) or the same medium without inhibitor. After 2 d, supernatant from the axon compartment was collected and directly used for ELISA. After fixation with 4% PFA for 30 min at room temperature, cell cultures were processed for immunocytochemical staining with antibodies against CXCL12 (1:250, R&D Systems, AB_2088149), GFP (1:1,000; Novus; RRID: AB_10128178), and βIII-tubulin (1:2,000; BioLegend, RRID: AB_2313773). Stained axons were photographed using a confocal microscope (630×, SP8, Leica).

ELISA. A sandwich ELISA was used to validate the secretion of CXCL12 from axons according to the manufacturer's protocol (Peprotech). In brief, wells of a 96-well plate were incubated with a CXCL12-specific capture antibody. After washing, the axonal compartments' supernatant and descending concentrations of recombinant CXCL12 were added to the wells. After 4 h of incubation and subsequent washing, wells were incubated with a biotinylated CXCL12-specific detection antibody for 2 h and washed again. After that, wells were incubated with HRP-conjugated avidin for 30 min, washed, and incubated with a 2,2'-azino-bis(3-ethylbenzothiazoline-6-sulfonic acid) (ABTS) solution. Each well's optic density was assessed at 405 nm using a Multiskan FC plate reader (ThermoFisher) with SkanIt for Multiskan FC 2.5.1 software. All conditions were measured in duplicates, and three independent experiments have been performed.

Western Blot of Retinal Lysates. Retinae from mice were collected after indicated treatments and lysed for Western blot analysis. Western blots were performed as described in the *SI Appendix*.

RNA Isolation and Quantitative Real-Time PCR. Total RNA was isolated from retinae with the vitreous body removed and optic nerves using the RNeasy Mini kit (Qiagen) according to the manufacturer's protocol. Tissue-derived RNA was reverse-transcribed using superscript II (Invitrogen). Expression analysis of *Cxcl12* and *Gapdh* was performed using SYBR Green PCR Master Mix (Applied Biosystems) and QuantiTect primers (Mm_Gapdh_3_SG and Mm_CXCL12_1_SG, Qiagen) on the Applied Biosystems 7500 real-time PCR system. The complementary DNA was amplified during 45 cycles according to the manufacturer's protocol. All reactions were performed in duplicate and for at least three independent runs. The specificity of the PCR products was verified with the dissociation curve analysis feature of the Applied Biosystems 7500 software.

Statistical Analysis. Normality and variance similarity was measured before we applied any statistical tests. Significances of intergroup differences with absolute values were evaluated using either Student's *t* test or one- or two-way ANOVA followed by Holm-Šídák post hoc test using GraphPad Prism software. The significances of intergroup differences with percentage data were evaluated using a χ^2 test with contingency tables using GraphPad Prism software. Error bars in all figures represent mean ± SEM. Mice with different litters, body weights, and sexes were randomized and assigned to different treatment groups, and no other specific randomization was used for the animal studies.

Data Availability. All study data are included in the article and/or supporting information.

1. J. L. Goldberg *et al.*, Retinal ganglion cells do not extend axons by default: Promotion by neurotrophic signaling and electrical activity. *Neuron* **33**, 689–702 (2002).
2. D. Fischer, Stimulating axonal regeneration of mature retinal ganglion cells and overcoming inhibitory signaling. *Cell Tissue Res.* **349**, 79–85 (2012).
3. D. Fischer, M. Leibinger, Promoting optic nerve regeneration. *Prog. Retin. Eye Res.* **31**, 688–701 (2012).
4. M. Berry, Z. Ahmed, A. Logan, Return of function after CNS axon regeneration: Lessons from injury-responsive intrinsically photosensitive and alpha retinal ganglion cells. *Prog. Retin. Eye Res.* **71**, 57–67 (2019).
5. D. Fischer, M. Pavlidis, S. Thanos, Cataractogenic lens injury prevents traumatic ganglion cell death and promotes axonal regeneration both in vivo and in culture. *Invest. Ophthalmol. Vis. Sci.* **41**, 3943–3954 (2000).
6. T. G. Hauk *et al.*, Stimulation of axon regeneration in the mature optic nerve by intravitreal application of the toll-like receptor 2 agonist Pam3Cys. *Invest. Ophthalmol. Vis. Sci.* **51**, 459–464 (2010).
7. Y. Yin *et al.*, Macrophage-derived factors stimulate optic nerve regeneration. *J. Neurosci.* **23**, 2284–2293 (2003).
8. A. Müller, T. G. Hauk, D. Fischer, Astrocyte-derived CNTF switches mature RGCs to a regenerative state following inflammatory stimulation. *Brain* **130**, 3308–3320 (2007).
9. M. Leibinger *et al.*, Neuroprotective and axon growth-promoting effects following inflammatory stimulation on mature retinal ganglion cells in mice depend on ciliary neurotrophic factor and leukemia inhibitory factor. *J. Neurosci.* **29**, 14334–14341 (2009).
10. M. Leibinger *et al.*, Interleukin-6 contributes to CNS axon regeneration upon inflammatory stimulation. *Cell Death Dis.* **4**, e609 (2013).
11. M. Leibinger, A. Andreadaki, D. Fischer, Role of mTOR in neuroprotection and axon regeneration after inflammatory stimulation. *Neurobiol. Dis.* **46**, 314–324 (2012).
12. M. Leibinger, A. Andreadaki, H. Diekmann, D. Fischer, Neuronal STAT3 activation is essential for CNTF- and inflammatory stimulation-induced CNS axon regeneration. *Cell Death Dis.* **4**, e805 (2013).
13. M. Leibinger *et al.*, Boosting CNS axon regeneration by harnessing antagonistic effects of GSK3 activity. *Proc. Natl. Acad. Sci. U.S.A.* **114**, E5454–E5463 (2017).
14. D. Fischer, Z. He, L. I. Benowitz, Counteracting the Nogo receptor enhances optic nerve regeneration if retinal ganglion cells are in an active growth state. *J. Neurosci.* **24**, 1646–1651 (2004).
15. V. Sengottuvel, M. Leibinger, M. Pfreimer, A. Andreadaki, D. Fischer, Taxol facilitates axon regeneration in the mature CNS. *J. Neurosci.* **31**, 2688–2699 (2011).
16. D. Fischer, V. Petkova, S. Thanos, L. I. Benowitz, Switching mature retinal ganglion cells to a robust growth state in vivo: Gene expression and synergy with RhoA inactivation. *J. Neurosci.* **24**, 8726–8740 (2004).
17. M. Leibinger, A. M. Hilla, A. Andreadaki, D. Fischer, GSK3-CRMP2 signaling mediates axonal regeneration induced by *Pten* knockout. *Commun. Biol.* **2**, 318 (2019).
18. A. Heskamp *et al.*, CXCL12/SDF-1 facilitates optic nerve regeneration. *Neurobiol. Dis.* **55**, 76–86 (2013).
19. O. Berger, G. Li, S. M. Han, M. Paredes, S. J. Pleasure, Expression of SDF-1 and CXCR4 during reorganization of the postnatal dentate gyrus. *Dev. Neurosci.* **29**, 48–58 (2007).
20. Q. Li *et al.*, Chemokine signaling guides axons within the retina in zebrafish. *J. Neurosci.* **25**, 1711–1717 (2005).
21. Y. Feng, C. C. Broder, P. E. Kennedy, E. A. Berger, HIV-1 entry cofactor: Functional cDNA cloning of a seven-transmembrane, G protein-coupled receptor. *Science* **272**, 872–877 (1996).
22. X. Sun *et al.*, CXCL12 / CXCR4 / CXCR7 chemokine axis and cancer progression. *Cancer Metastasis Rev.* **29**, 709–722 (2010).
23. L. Cui *et al.*, Stromal cell-derived factor-1 and its receptor CXCR4 in adult neurogenesis after cerebral ischemia. *Restor. Neurol. Neurosci.* **31**, 239–251 (2013).
24. T. Pozzobon, G. Goldoni, A. Viola, B. Molon, CXCR4 signaling in health and disease. *Immunol. Lett.* **177**, 6–15 (2016).
25. K. Tashiro *et al.*, Signal sequence trap: A cloning strategy for secreted proteins and type I membrane proteins. *Science* **261**, 600–603 (1993).
26. C. C. Bleul, R. C. Fuhlbrigge, J. M. Casasnovas, A. Aiuti, T. A. Springer, A highly efficacious lymphocyte chemoattractant, stromal cell-derived factor 1 (SDF-1). *J. Exp. Med.* **184**, 1101–1109 (1996).
27. X. Luo *et al.*, Crosstalk between astrocytic CXCL12 and microglial CXCR4 contributes to the development of neuropathic pain. *Mol. Pain* **12**, 1744806916636385 (2016).
28. B. M. Woerner, N. M. Warrington, A. L. Kung, A. Perry, J. B. Rubin, Widespread CXCR4 activation in astrocytomas revealed by phospho-CXCR4-specific antibodies. *Cancer Res.* **65**, 11392–11399 (2005).
29. M. Krumbholz *et al.*, Chemokines in multiple sclerosis: CXCL12 and CXCL13 upregulation is differentially linked to CNS immune cell recruitment. *Brain* **129**, 200–211 (2006).

10 of 11 | PNAS
https://doi.org/10.1073/pnas.2016409118

Hilla et al.
CXCR4/CXCL12-mediated entrapment of axons at the injury site compromises optic nerve regeneration

30. R. K. Stumm et al., A dual role for the SDF-1/CXCR4 chemokine receptor system in adult brain: Isoform-selective regulation of SDF-1 expression modulates CXCR4-dependent neuronal plasticity and cerebral leukocyte recruitment after focal ischemia. J. Neurosci. 22, 5865–5878 (2002).

31. A. Zlotnik, O. Yoshie, H. Nomiyama, The chemokine and chemokine receptor superfamilies and their molecular evolution. Genome Biol. 7, 243 (2006).

32. S. H. Chalasani, K. A. Sabelko, M. J. Sunshine, D. R. Littman, J. A. Raper, A chemokine, SDF-1, reduces the effectiveness of multiple axonal repellents and is required for normal axon pathfinding. J. Neurosci. 23, 1360–1371 (2003).

33. X. Duan et al., Subtype-specific regeneration of retinal ganglion cells following axotomy: Effects of osteopontin and mTOR signaling. Neuron 85, 1244–1256 (2015).

34. D. Fischer, A. R. Harvey, V. Pernet, V. P. Lemmon, K. K. Park, Optic nerve regeneration in mammals: Regenerated or spared axons? Exp. Neurol. 296, 83–88 (2017).

35. V. Grozdanov, A. Muller, V. Sengottuvel, M. Leibinger, D. Fischer, A method for preparing primary retinal cell cultures for evaluating the neuroprotective and neuritogenic effect of factors on axotomized mature CNS neurons. Curr. Protoc. Neurosci. 53, 3.22.1–3.22.10(2010).

36. A. Marchese et al., The E3 ubiquitin ligase AIP4 mediates ubiquitination and sorting of the G protein-coupled receptor CXCR4. Dev. Cell 5, 709–722 (2003).

37. P. G. Hirrlinger, A. Scheller, C. Braun, J. Hirrlinger, F. Kirchhoff, Temporal control of gene recombination in astrocytes by transgenic expression of the tamoxifen-inducible DNA recombinase variant CreERT2. Glia 54, 11–20 (2006).

38. A. M. Hilla, H. Diekmann, D. Fischer, Microglia are irrelevant for neuronal degeneration and axon regeneration after acute injury. J. Neurosci. 37, 6113–6124 (2017).

39. B. A. Rheaume et al., Single cell transcriptome profiling of retinal ganglion cells identifies cellular subtypes. Nat. Commun. 9, 2759 (2018).

40. D. T. Akin, J. M. Kinkade Jr, R. T. Parmley, Biochemical and ultrastructural effects of monensin on the processing, intracellular transport, and packaging of myeloperoxidase into low and high density compartments of human leukemia (HL-60) cells. Arch. Biochem. Biophys. 257, 451–463 (1987).

41. J. Lippincott-Schwartz, L. C. Yuan, J. S. Bonifacino, R. D. Klausner, Rapid redistribution of Golgi proteins into the ER in cells treated with brefeldin A: Evidence for membrane cycling from Golgi to ER. Cell 56, 801–813 (1989).

42. A. Reaux-Le Goazigo, C. Rivat, P. Kitabgi, M. Pohl, S. Melik Parsadaniantz, Cellular and subcellular localization of CXCL12 and CXCR4 in rat nociceptive structures: Physiological relevance. Eur. J. Neurosci. 36, 2619–2631 (2012).

43. K. K. Park et al., Promoting axon regeneration in the adult CNS by modulation of the PTEN/mTOR pathway. Science 322, 963–966 (2008).

44. M. Leibinger et al., Boosting central nervous system axon regeneration by circumventing limitations of natural cytokine signaling. Mol. Ther. 24, 1712–1725 (2016).

45. M. Leibinger et al., Transneuronal delivery of hyper-interleukin-6 enables functional recovery after severe spinal cord injury in mice. Nat. Commun. 12, 391 (2021).

46. A. Guyon, CXCL12 chemokine and its receptors as major players in the interactions between immune and nervous systems. Front. Cell. Neurosci. 8, 65 (2014).

47. S. Heinisch, L. G. Kirby, SDF-1alpha/CXCL12 enhances GABA and glutamate synaptic activity at serotonin neurons in the rat dorsal raphe nucleus. Neuropharmacology 58, 501–514 (2010).

48. K. Reiss, R. Mentlein, J. Sievers, D. Hartmann, Stromal cell-derived factor 1 is secreted by meningeal cells and acts as chemotactic factor on neuronal stem cells of the cerebellar external granular layer. Neuroscience 115, 295–305 (2002).

49. T. G. Hauk, A. Müller, J. Lee, R. Schwendener, D. Fischer, Neuroprotective and axon growth promoting effects of intraocular inflammation do not depend on oncomodulin or the presence of large numbers of activated macrophages. Exp. Neurol. 209, 469–482 (2008).

50. A. R. Sas et al., A new neutrophil subset promotes CNS neuron survival and axon regeneration. Nat. Immunol. 21, 1496–1505 (2020).

51. A. Guyon et al., Complex effects of stromal cell-derived factor-1 alpha on melanin-concentrating hormone neuron excitability. Eur. J. Neurosci. 21, 701–710 (2005).

52. Q. Ma et al., Impaired B-lymphopoiesis, myelopoiesis, and derailed cerebellar neuron migration in CXCR4- and SDF-1-deficient mice. Proc. Natl. Acad. Sci. U.S.A. 95, 9448–9453 (1998).

53. M. Lu, E. A. Grove, R. J. Miller, Abnormal development of the hippocampal dentate gyrus in mice lacking the CXCR4 chemokine receptor. Proc. Natl. Acad. Sci. U.S.A. 99, 7090–7095 (2002).

54. F. Pujol, P. Kitabgi, H. Boudin, The chemokine SDF-1 differentially regulates axonal elongation and branching in hippocampal neurons. J. Cell Sci. 118, 1071–1080 (2005).

55. T. Netelenbos et al., Proteoglycans on bone marrow endothelial cells bind and present SDF-1 towards hematopoietic progenitor cells. Leukemia 17, 175–184 (2003).

56. E. R. Bray et al., 3D visualization of individual regenerating retinal ganglion cell axons reveals surprisingly complex growth paths. eNeuro 4, ENEURO.0093-17.2017 (2017).

57. J. Peng et al., Sonic hedgehog is a remotely produced cue that controls axon guidance trans-axonally at a midline choice point. Neuron 97, 326–340.e4 (2018).

58. A. R. Filous et al., Entrapment via synaptic-like connections between NG2 proteoglycan+ cells and dystrophic axons in the lesion plays a role in regeneration failure after spinal cord injury. J. Neurosci. 34, 16369–16384 (2014).

59. D. Schols, J. A. Esté, G. Henson, E. De Clercq, Bicyclams, a class of potent anti-HIV agents, are targeted at the HIV coreceptor fusin/CXCR-4. Antiviral Res. 35, 147–156 (1997).

60. X. Luo et al., Three-dimensional evaluation of retinal ganglion cell axon regeneration and pathfinding in whole mouse tissue after injury. Exp. Neurol. 247, 653–662 (2013).

61. F. Sun et al., Sustained axon regeneration induced by co-deletion of PTEN and SOCS3. Nature 480, 372–375 (2011).

62. A. M. Hilla, D. Fischer, Studying the role of microglia in neurodegeneration and axonal regeneration in the murine visual system Bio-Protoc. 8, e2979 (2018).

63. N. Renier et al., iDISCO: A simple, rapid method to immunolabel large tissue samples for volume imaging. Cell 159, 896–910 (2014).

64. P. Gobrecht, M. Leibinger, A. Andreadaki, D. Fischer, Sustained GSK3 activity markedly facilitates nerve regeneration. Nat. Commun. 5, 4561 (2014).

65. E. Levin, H. Diekmann, D. Fischer, Highly efficient transduction of primary adult CNS and PNS neurons. Sci. Rep. 6, 38928 (2016).

NEUROSCIENCE

Hilla et al.
CXCR4/CXCL12-mediated entrapment of axons at the injury site compromises optic nerve regeneration

PNAS | 11 of 11
https://doi.org/10.1073/pnas.2016409118